Microsc. Microanal. 17, 903–910, 2011
doi:10.1017/S1431927611012189

Microscopy AND Microanalysis

Compton Scattering Artifacts in Electron Excited X-Ray Spectra Measured with a Silicon Drift Detector

Nicholas W.M. Ritchie,* Dale E. Newbury, and Abigail P. Lindstrom

National Institute of Standards and Technology, Gaithersburg, MD 20899, USA

Abstract: Artifacts are the nemesis of trace element analysis in electron-excited energy dispersive X-ray spectrometry. Peaks that result from nonideal behavior in the detector or sample can fool even an experienced microanalyst into believing that they have trace amounts of an element that is not present. Many artifacts, such as the Si escape peak, absorption edges, and coincidence peaks, can be traced to the detector. Others, such as secondary fluorescence peaks and scatter peaks, can be traced to the sample. We have identified a new sample-dependent artifact that we attribute to Compton scattering of energetic X-rays generated in a small feature and subsequently scattered from a low atomic number matrix. It seems likely that this artifact has not previously been reported because it only occurs under specific conditions and represents a relatively small signal. However, with the advent of silicon drift detectors and their utility for trace element analysis, we anticipate that more people will observe it and possibly misidentify it. Though small, the artifact is not inconsequential. Under some conditions, it is possible to mistakenly identify the Compton scatter artifact as approximately 1% of an element that is not present.

Key words: Compton scatter, silicon drift detector (SDD), energy dispersive, Monte Carlo, X-ray, electron probe microanalysis (EPMA), artifacts

Introduction

Trace element analysis via electron probe X-ray microanalysis is always a challenge. Traditionally, trace element analysis has been the purview of wavelength dispersive spectrometry (WDS) on dedicated electron microprobes. However, with the advent of the silicon drift detector (SDD), it is possible to collect energy dispersive spectra with count statistics approaching or exceeding those of wavelength dispersive spectrometers with similar electron dose and acquisition times (albeit with less optimal peak-to-background ratios). As a result, SDDs are likely to be used more frequently for performing trace element analysis. However, with these excellent count statistics and the trace signal size, small measurement artifacts become increasingly significant. Operating with the same basic detection physics, SDDs are susceptible to the same artifacts that plague traditional lithium drifted silicon [Si(Li)] detectors (Goldstein et al., 2003).

SDDs are more susceptible to Si escape peaks because they are typically about six times thinner than Si(Li) detectors. Si escape peaks occur when a characteristic X-ray is absorbed by the detector, but the resulting ionization relaxes via a Si K X-ray that escapes the detection volume. Absorption edge artifacts are created in the bremsstrahlung (continuum) background at ionization energies by elements present in the detector crystal and window. Instrument peak artifacts, which are due to scattered electrons striking materials in the instrument chamber, are particularly difficult to characterize because they depend strongly on variations in the specimen topography. Coincidence peak artifacts, which are due to near simultaneous detection of multiple X-rays, develop at higher throughput. Coincidence peaks are a particular challenge because they often present themselves at energies that mimic or interfere with peaks from elements of interest. The incomplete charge collection artifact, a low energy tail on characteristic peaks, remains a problem for some vendor's design of SDDs but has been much mitigated in others by minimizing the partially dead layer, a thin insensitive layer on the front face of the detector crystal. Incomplete charge collection is typically more of a problem at lower energies ($\ll$10 keV) and can be checked by observing the deviation from Gaussian line shape on the low energy side of characteristic peaks.

Other artifacts are produced by the sample. Since the range of X-rays typically far exceeds the range of electrons in the sample, it is possible for X-rays to generate secondary fluorescence from elements in remote regions that never interact with the electron beam. If the sample is small relative to the mean X-ray path length, then the X-rays can escape the sample volume and be absorbed by surrounding materials. These materials will produce characteristic X-rays that can be detected. Particularly on topographically complex samples, back- and sidescattering of the incident electron beam can also lead to unanticipated element peaks from remote materials.

We believe that we have identified a new sample dependent artifact that we attribute to Compton scattering, the

Disclaimer: Certain commercial equipment, instruments, or materials are identified in this article to foster understanding. Such identification does not imply recommendation or endorsement by the National Institute of Standards and Technology, nor does it imply that the materials or equipment identified are necessarily the best available for the purpose.

Received November 17, 2010; accepted July 7, 2011
*Corresponding author. E-mail: nicholas.ritchie@nist.gov

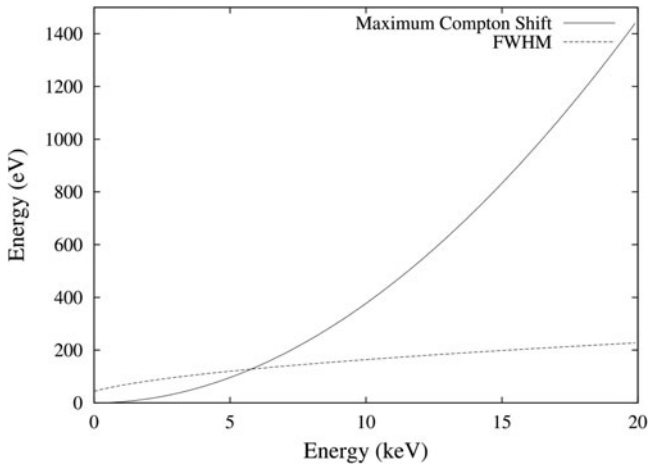

Figure 1. The maximum ($\theta = \pi$) Compton shift as a function of incident photon energy as computed using Klein-Nishina's theory. The photon may scatter through an angle less than π and lose less energy. The Compton shift is compared with the FWHM for an X-ray detector with a nominal FWHM of 129 eV at manganese Kα.

incoherent scattering of energetic photons from electrons (Compton, 1923). Arthur Holly Compton received the 1927 Nobel Prize in Physics for this discovery. Compton scattering is of particular interest because it cannot be explained by classical wave-based electrodynamics. Light must be quantized to explain the occurrence of the Compton process at arbitrarily low radiation fluxes. The first theoretical model (Klein & Nishina, 1928) was one of the early accomplishments of the then new quantum electrodynamics.

Klein and Nishina treat the photon and electron as a two-body problem in which both energy and momentum must be conserved. In their simple model, the electron is assumed to be at rest and unbound. The energy loss in a Compton event is a function of the deflection angle, θ, between the incoming and outgoing X-ray.

$$E'_\gamma = \frac{E_\gamma}{1 + \dfrac{E_\gamma}{m_e c^2}\,(1 - \cos(\theta))}. \tag{1}$$

The constant $m_e c^2 = 511$ keV represents the rest-mass of an electron. For example, a 13.6 keV U L3-M5 photon will lose 0.69 keV when it is scattered through π radians. Figure 1 shows the maximum Compton shift (which always occurs at $\theta = \pi$) as a function of incident photon energy for the range of energies of interest to microanalysts.

Photons in the range of energies associated with electron probe microanalysis (EPMA) interact primarily with the atomic electrons. Three types of interactions dominate at these energies—photoelectric absorption, Rayleigh (coherent) scattering, and Compton (incoherent) scattering (Markowicz, 2002).

Photoelectric absorption involves an X-ray photon transferring all its energy to the electrons in an atom. The atom is ionized, and an energetic electron is emitted. In the range of photon energy typically involved in EPMA, photoabsorption is the dominant process. Photoabsorption is usually the principal effect that we correct for when we perform $\phi(\rho \cdot z)$ or $Z \cdot A \cdot F$ corrections. Figure 2 shows the photoabsorption cross section for carbon, strontium, and uranium (Chantler et al., 2005).

Rayleigh scattering is the coherent, elastic scattering of photons. Rayleigh scattering changes the direction of the X-ray trajectory but not the energy. We are most familiar with the Rayleigh process as the process that makes the sky blue. Because Rayleigh scattering does not involve any energy loss, we will not observe a distinct artifact peak. It is possible, however, that Rayleigh scattering may diminish the measured intensity particularly in WDS measurements. Photons, which are Rayleigh scattered, on a trajectory to the detector may not reach the detector leading to diminished measured intensity. However, on detectors with large acceptance angles [like most energy dispersive spectrometer (EDS) detectors], this effect is largely compensated by photons whose initial trajectory would not strike the detector but are Rayleigh scattered into the detector. WDS detectors typically have small detection volumes and tight acceptance angles. In this case, the compensation mechanism will not work as efficiently, and Rayleigh scattering can result in a loss of measured intensity.

Compton scattering is the third interaction type. Like Rayleigh scattering, the cross section for the Compton scattering is typically much smaller than the cross section for photoelectric absorption. Only at high photon energies ($>$10 keV) in low atomic number materials are the Compton, Rayleigh, and the photoelectric absorption processes of similar magnitude. Furthermore, we would never resolve the Compton process as a distinct artifact peak unless the energy separation between the artifact and the peak exceeds the detector resolution expressed as full-width at half-maximum (FWHM) by approximately a factor of 2. Figure 1 compares the Compton shift to the FWHM of a typical SDD, suggesting that a source of hard X-rays ($>$12 keV) is needed to observe the artifact. This could be the K line of an element with $Z \geq 35$ or the L line of an element with $Z \geq 87$.

These two properties of the Compton process suggest why the phenomenon has not been previously observed in EPMA spectra. Low atomic number materials do not produce sufficiently energetic X-rays for either the cross section to be sufficiently large or for the energy shift to be large enough to resolve with EDS. High atomic number materials produce sufficiently energetic X-rays, but the Compton cross section is small compared to the absorption process, and so the signal is lost in the bulk target. These criteria do suggest that Compton scattering might be observed when energetic X-rays produced by a high atomic number material are subsequently scattered from a low atomic number substrate. This circumstance is not uncommon in particle or inclusion analysis. A higher atomic number particle or inclusion can produce energetic X-rays that escape the volume of the source and interact with a low atomic num-

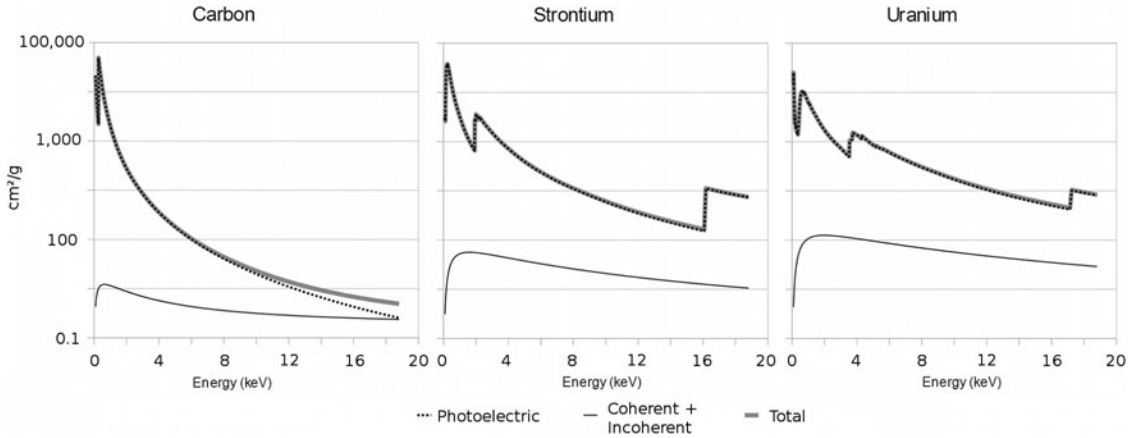

Figure 2. Mass attenuation coefficients from the FFAST database for the elements carbon, strontium, and uranium (Chantler et al., 2005).

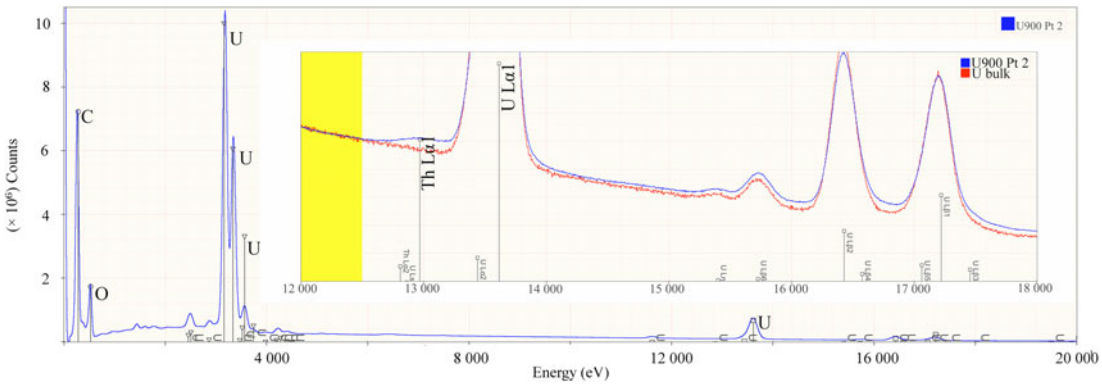

Figure 3. Electron excited energy dispersive X-ray spectra from particles of high purity U_3O_8. The inset plot emphasizes the range of energies around 10 to 20 keV with an enhanced vertical scale to show the U Lα family. We suggest that the peak labeled with the thorium Lα1 marker is not in fact thorium but rather an artifact due to Compton scattering. A spectrum from bulk U_3O_8 is plotted for comparison.

ber substrate. Some of the most common substrates for particle analysis (carbon, beryllium, and boron) turn out to be ideal for observing the Compton process.

Materials and Methods

The experiments were performed on a JEOL (Tokyo, Japan) JXA-8500F microprobe at a beam energy of 30 keV using a Bruker 4040 SDD (Bruker, Karlsruhe, Germany). The Bruker 4040 is a single head containing four independent SDDs, each with an independent pulse processor. The pulse processors were configured with a time constant of 400 ns that produces a resolution of 127.9 ± 0.3 eV FWHM at Mn Kα. A probe current of 5 nA was chosen to balance the conflicting goals of (1) collecting a high count spectrum and (2) minimizing coincidence events. 5 nA produces about 80–100k counts/s from four distinct detectors or approximately 20–25k counts/s per detector. This moderate count rate for this detector at this pulse process time produces a dead time of approximately 10%. The spectra were acquired for 5,000 s, which produced an integrated count of approximately 5×10^6 X-ray events in each particle spectrum.

The first material we investigated was U_3O_8 particles from NIST (National Institute of Standards and Technology, Gaithersburg, MD, USA) SRM-U900 (Uriano, 1981) mounted on a pyrolytic carbon substrate. While in general accurate quantitative analysis of particles is difficult, we wanted to estimate the maximum amount of Th in our sample based on the ratio of the U L to Th L line intensities. We measured the spectra shown in Figure 3 from two particles labeled "U900 point 3" and "U900 point 4." The main plot shows the spectrum from 0 to 20 keV. The inset spectrum shows the same spectrum except the horizontal scale is limited to 12 to 18 keV, and the vertical scale is limited to approximately 3×10^5 counts. The plots are labeled with characteristic X-ray lines for uranium and thorium. When we performed standards-based quantitative analysis on these spectra, the residuals derived from multiple linear least-squares fitting using DTSA-II (Ritchie, 2010) from the uranium peaks were good. However, when we tried to fit the peak labeled thorium Lα1 with a high quality, high count thorium standard, the fit was poor. Investigations showed that the peak could not be accounted for by a single element or superposition of elements. Fur-

thermore, both mass spectrometry measurements made by colleagues and the SRM certificate confirmed that the particle contained at least two orders of magnitude less thorium than our standards-based quantification suggested. Upon further investigation we determined that the peak could not be a Th Lα line, a Pa L line, a Kr K line, or a Rb K line. Nor could we identify any established artifact to which the peak could be attributed.

Residual spectra, the derived spectrum constructed from the original spectrum minus the reference spectrum's characteristic peaks scaled by the k-ratios, are very powerful tools for determining whether the peaks in the spectrum have been accounted for correctly. A clean residual looks like a bremsstrahlung-only spectrum—characteristic peaks are absent except maybe for a region of higher than typical channel noise. A classic example of the power of the residual is benitiote—$BaTSi_3O_9$. A common mistake is to overlook the Ti because the Ti K lines are obscured by the Ba L lines. If you fit benitoite with Ba, Si, and O, the residual in the region of the Ba L lines will retain nonbremsstrahlung-like structure. Another example of the power of the residual is as a diagnostic for the mistake of fitting Th M as Ag L. The residual of a thorium spectrum fit as silver will show additional structure because even though the Th M and Ag L peaks overlap almost perfectly, the line shapes are subtley different. The residual is such an important diagnostic that DTSA-II always computes one each time a spectrum is quantified. In this case, the residual from the Compton scatter feature fit as Th or any other combination of candidate elements always looked poor suggesting that something else was happening.

To follow up on this initial observation, we performed the following experiments to investigate the relationship between the substrate and the artifact and to see whether it was unique to uranium or the L-family of characteristic X-rays. We mounted particles with a high atomic number constituent (SrF_2) on a 3.7 μm thick Mylar film suspended above a void (see Fig. 4A). The configuration was designed to approximate as close as possible an unsupported particle in free space. Mylar film is essentially transparent to energetic electrons and X-rays. The direct line-of-sight from the base of the void to the detector was obstructed so that electrons that scattered through the Mylar and struck the supports under the void would not produce measured X-rays. We measured spectra from the particles. Then we placed various different substrates immediately under the Mylar film, including two thicknesses of carbon (3 and 6 mm) and an aluminum disk.

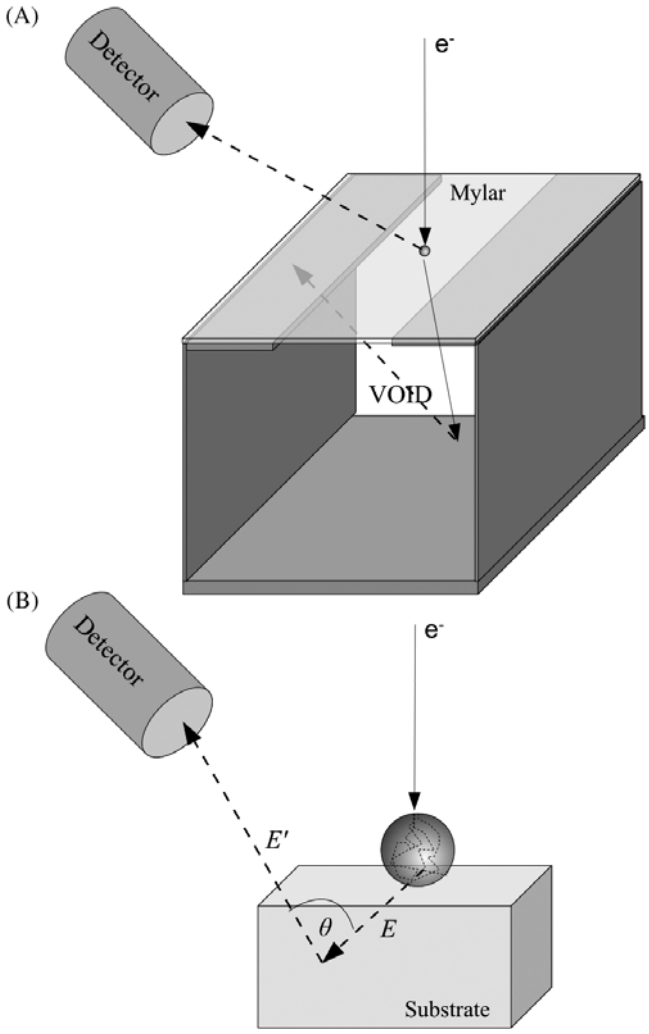

Figure 4. A: A schematic diagram showing the process leading to a Compton artifact. An electron beam generates an energetic characteristic X-ray of energy E in a volume of matter small compared to the mean X-ray absorption path length. The characteristic X-ray propagates out of the volume and into a substrate with absorption and Compton cross sections of similar magnitude. The characteristic X-ray Compton scatters by an angle θ off an electron in the substrate. The resulting photon of energy $E'(E, \theta)$ propagates to the detector. The position of the sample, the Compton scatter event, and the detector define a narrow range of scatter angles (θ) for the detected photons. **B:** A schematic diagram showing how the Mylar suspended the particle over a void. The depth of the void and the angle of the detector minimize the number of scattered or otherwise undesired X-rays.

Results

Figure 5 shows four different spectra collected from the same SrF_2 particle supported on a 3.7 μm Mylar film. The spectrum collected when only the Mylar is present looks exactly as we would expect for bulk SrF_2. The regions on the low energy side of the Kα and Kβ peaks show only the expected bremsstrahlung background. This is also true for the spectrum collected with the aluminum disk positioned directly under the film. The Mylar-only and the Mylar-over-Al spectra are virtually indistinguishable. However, the two spectra collected over the carbon planchets show an additional peak on the low energy side of the Kα and Kβ peaks. The thick carbon planchet shows the largest artifact. The artifact is visible on the low energy side of both the Kα and Kβ peaks although the magnitude is larger on the Kα by approximately the ratio of the Kα intensity to Kβ intensity. The artifact is present with the 3 mm thick carbon

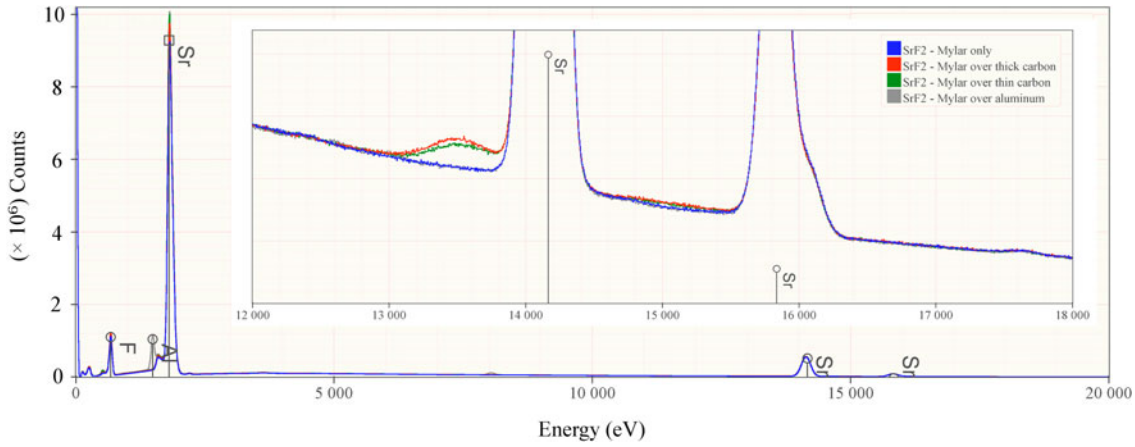

Figure 5. Four spectra collected from one SrF_2 particle mounted on a 3.7 μm Mylar film and suspended over a void. The spectra differ in the material placed in the void immediately under the Mylar film. In order from the top of the legend, the first spectrum has nothing mounted in the void. The next three have, respectively, 6 mm of carbon, 3 mm of carbon, and 6 mm of aluminum. The spectra overlap almost perfectly in the overview, but it is possible to see a small Al peak in the Mylar over Al spectrum from electrons scattered out of the particle and secondary fluorescence.

planchet but is ≈20% less intense than the 6 mm thick carbon planchet.

Similar experiments (results not shown) performed using U900 particles on a carbon support transmission electron microscope grid produced similar results—no artifact when there was no substrate under the grid and an artifact when a carbon planchet was placed under the grid. These results are more difficult to model due to the proximity of the copper grid, so we will focus on the SrF_2 on Mylar.

Discussion

The experimental results present various observations that require explanation:

- the presence of an artifact when a SrF_2 or U_3O_8 particle is mounted over a carbon substrate
- the variation in intensity of the artifact with the thickness of the carbon substrate
- the absence of the artifact when the particle is suspended on a thin film
- the absence of the artifact when the particle is mounted over an aluminum substrate
- the absence of the artifact in bulk samples
- the shape and position of the artifact
- the approximate magnitude of the artifact.

The proposed mechanism is shown in Figure 4B. Energetic characteristic X-rays are generated in a small volume of matter (particle or inclusion). The volume must be small enough that a substantial fraction of the X-rays will escape toward the substrate. The ideal volume is probably about the electron interaction volume because this volume maximizes the primary signal but also has a relatively small absorption path length. The substrate can Rayleigh scatter, Compton scatter, or photoabsorb photons. If a large fraction of photons are photoabsorbed, then a small fraction remains to Compton scatter. Furthermore, if a large fraction of the photons that do Compton scatter are photoabsorbed, then a small fraction remains to be detected. This suggests that if the photoabsorption cross section is much larger than the Compton scattering cross section, the artifact will be greatly diminished and is unlikely to be visible. The only set of circumstances common in microanalysis for which the Compton scattering cross section is comparable to the absorption cross section is for photons with X-ray energies substantially above 10 keV interacting with a low atomic number substrate.

The length scales relevant to the Compton process are long. Table 1 lists the relevant cross sections for carbon, oxygen, strontium, and aluminum. In carbon with a nominal density of 2.3 g/cm^3, the mean absorption path length and mean Compton path length for Sr Kα are, respectively, 7 and 28 mm. These are three or four orders of magnitude larger than typical electron interaction volumes. A 3.7 μm Mylar film is not going to absorb or scatter many X-rays and is thus essentially transparent for the purposes of this experiment. However, the two different carbon substrate

Table 1. Cross Sections for Various X-Ray Processes Including Photoabsorption, Rayleigh and Compton Scattering for the Elements Carbon, Oxygen, Aluminum, and Strontium at the Strontium Kα1 Energy (E = 14.165 keV).*

Element	Photoelectric (cm^2/g)	Coherent (Rayleigh) (cm^2/g)	Incoherent (Compton) (cm^2/g)
C	0.593	0.107	0.156
O	1.714	0.174	0.148
Al	8.877	0.250	0.120
Sr	22.047	1.357	0.083

*The calculations are based on the data compiled by McMaster et al. (1969) as implemented by P. Bandyopadhyay and C.U. Segre (available at www.csrri.iit.edu/mucal.html).

thicknesses are of the correct length scales both to produce the artifact and to show differences due to thickness. The mean path length for photoabsorption is four times larger than the mean path length for Compton scattering. Thus most photons will be photoabsorbed, but a nonnegligible fraction will be Compton scattered. A significant fraction of the scattered photons is also likely to be able to escape to the detector without being photoabsorbed.

The aluminum substrate is a different story. At a nominal density of 2.7 g/cm^3, the mean photoabsorption and mean Compton path lengths for Sr Kα are 0.4 and 30 mm, respectively. Characteristic photons are 75 times more likely to be absorbed than to scatter. Furthermore, those that do scatter are likely to be absorbed before they reach the detector. As a result, the Compton artifact is so diminished that we do not observe it.

The story is similar for bulk SrF_2. At a nominal density of 4.24 g/cm^3, the mean photoabsorption and mean Compton path lengths for Sr Kα are 0.15 and 24 mm, respectively. Using similar reasoning we do not expect to see a Compton artifact in bulk SrF_2 or bulk U_3O_8.

A Compton scattering artifact has been reported in spectra from analytical electron microscopes (AEM) (Wilson & Lambrianidis, 1990). In this case, the sources of the X-ray are the molybdenum column apertures, and the scatter is from a carbon insert in the upper objective lens pole piece. The AEM artifact is always present at the same energy independent of sample. Furthermore, the AEM artifact is more sharply peaked because the X-ray source and detector positions select a single scatter angle and thus a single Compton energy. The AEM artifact is essentially an artifact of a specific instrument's design, whereas the artifact we are reporting is more significant because it is due to the sample and under the right conditions it will presumably be present in any instrument.

Compton scattering artifacts are also common in X-ray fluorescence (XRF) spectra. In this case, the source of the primary X-ray is the X-ray tube. Since the angle between the X-ray tube, the sample, and the detector is fixed and constrained to a relatively small range of values, the Compton artifact leads most visibly to a series of peaks corresponding to the tube anode material but shifted to lower energy. These X-rays represent a structured background that can make interpreting XRF spectra more difficult.

A Monte Carlo Model of Compton Scattering

Understanding the shape and magnitude of the artifact relative to the primary peak requires a more sophisticated model than described above. We extended the Monte Carlo simulation in NIST DTSA-II (Ritchie, 2010) to model the trajectory of characteristic photons generated in a particle that escapes into a substrate material. The Monte Carlo assumes that the characteristic photons are emitted isotropically from the particle. The initial propagation direction of the photon is selected at random (Knop, 1970). Approximately half will propagate away from the substrate, and a small fraction of these will be measured directly by the detector. The other half will propagate into the substrate where they may either be photoabsorbed or Compton scattered. The mean-free-path for Compton scattering is computed using the algorithm in the Fortran source file MUCAL.F (program provided by P. Bandyopadhyay and C.U. Segre in 2005; available at www.csrri.iit.edu/mucal.html), which is based on McMasters' report (McMaster et al., 1969). From the mean-free-paths for these processes, we select random deviates from the exponential distribution to model an ensemble of absorption/Compton path lengths. For each characteristic X-ray, the smaller of the Compton or absorption paths is deemed to occur. If the absorption process occurs, the iteration ends and we proceed to the next characteristic photon. If the Compton process occurs, we calculate the angle θ that would scatter the characteristic photon into the detector. The angle θ determines the energy of the Compton scattered photon. The Compton process is not isotropic but for an incident photon of energy E_γ can be expressed in terms of the differential cross section as

$$\frac{d\sigma}{d\Omega} = \frac{1}{2}\alpha^2 r_c^2 P(E_\gamma,\theta)^2 \times \left(P(E_\gamma,\theta) + \frac{1}{P(E_\gamma,\theta)} - 1 + \cos^2(\theta)\right), \quad (2)$$

where $\alpha = e^2/\hbar c 4\pi\varepsilon_0$ is the fine structure constant, $r_c = \hbar m_e c$ is the Compton radius of the electron, m_e is the mass of an electron, and $P(E_\gamma,\theta)$ is the ratio of photon energy after and before the collision,

$$P(E_\gamma,\theta) = \frac{1}{1 + \frac{E_\gamma}{m_e c^2}(1 - \cos(\theta))}. \quad (3)$$

The energy ranges of interest to microanalysts are small compared to the rest energy of the electron. At these energies the relativistic effects are negligible and the differential cross section is approximately

$$\frac{d\sigma}{d\Omega} = \frac{1}{2}\alpha^2 r_c^2 (1 + \cos^2(\theta)). \quad (4)$$

We scale the scattered intensity to account for the differential cross section.

A fraction of the scattered X-rays will propagate toward the detector. Some of these will be absorbed by the intervening sample material. We account for this using the Beer-Lambert Law using the Form Factor, Attenuation, and Scattering Tables (FFAST) mass absorption coefficients (Chantler et al., 2005). We also account for the detection volume by discarding all primary photons that travel more than 1 cm from the optimal detection point (on the beam axis at the optimal working distance for the detector) except those that are propagating to the detector. The characteristic and Compton photons are accumulated and then convolved to emulate the resolution of the detector.

The results of the model are shown in Figure 6 for both U_3O_8 and SrF_2. The agreement is rough. The model is

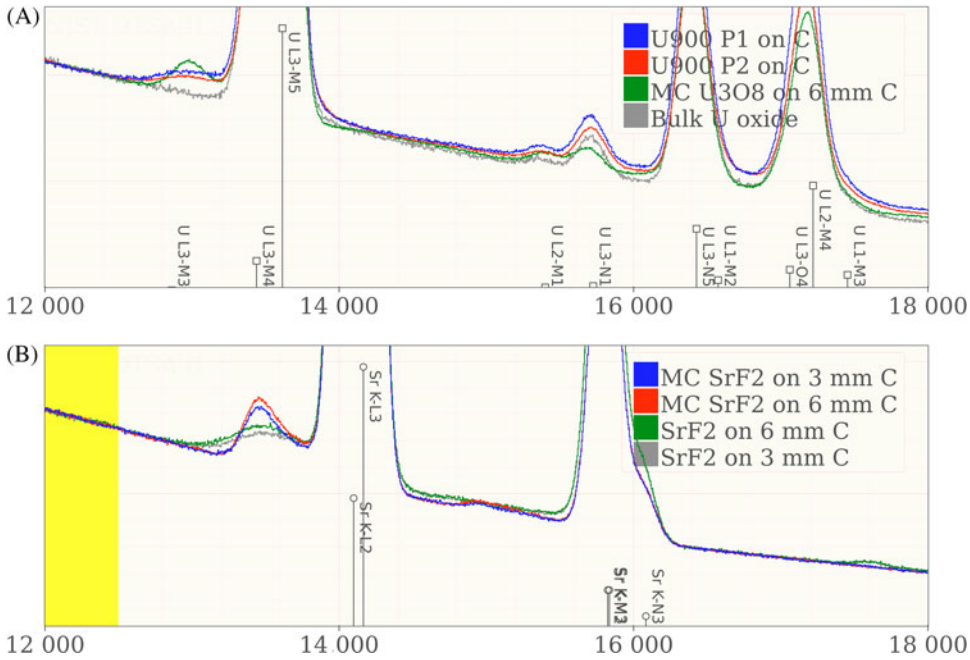

Figure 6. Comparing Monte Carlo simulated spectra with measured spectra for (**A**) U_3O_8 and (**B**) SrF_2 particles on carbon substrates. The U_3O_8 spectra compare two different particle spectra with a bulk U oxide spectrum and a simulated U_3O_8 spectrum with simulated Compton scattering. The particulate and bulk spectra are distinctly different in the region below the L3-M5 (Lα) peak. This peak is accounted for in the Monte Carlo simulation, which accounts for Compton scattering from the carbon substrate. The SrF_2 spectra demonstrate the same process in SrF_2 particles on two different thicknesses of C. All the spectra are scaled to an equal integral in the 12.00 to 12.5 keV region. The simulated spectra match the intensity of the Compton feature reasonable well, which is to say that the total cross section is approximately correct. However, the shape that results from the actual energy shift does not match as well. This is likely due to the simple Compton model used that assumes unbound electrons at rest.

clearly more sharply peaked than the measured. However, the integrated intensity is approximately correct. The disparity in the shape may be due to the simple model for the differential cross section expressed in equation (2). This expression was derived for a stationary, unbound electron. An electron in a material satisfies neither criteria (Salvat et al., 2009). The atomic and solid state binding energies limit the number of electrons that can take part in Compton event to those bound by less energy than the energy shift. Second, the electrons are not stationary and thus see a Doppler shifted incident photon energy.

Conclusion

Silicon drift detectors show a lot of promise for extending the range of range of quantitative analysis with an energy dispersive detector further into the trace regime. However, SDDs must be used with care. There are many artifacts that are present with an SDD that are not present with a WDS detector. The Compton artifact though a rarity compared to escape and coincidence artifacts is one such example. We do not anticipate seeing the Compton artifact on wavelength dispersive spectrometers for two reasons. First, the detection volume for a WDS is much smaller as a result of the focusing characteristics of the spectrometer than the detection volume for an SDD, and the scatter volume for the Compton process is large. Second, the Compton artifact is a dispersive artifact and does not represent a sharp, well-defined line. Ignoring the previous argument about detection volume, the ratio of the intensity of the Compton artifact to the intensity of the bremsstrahlung background should be the same at a fixed energy on the wavelength or at a channel of equivalent (albeit broader) energy on an EDS. However, because the peak-to-background is higher on a wavelength spectrometer, the magnitude of the Compton artifact relative to the magnitude of the peak will be much smaller. With sufficient patience to collect sufficient counts in the background region, it might be possible to see the artifact in wavelength spectra.

The Compton artifact can be anticipated when a particle or inclusion producing an energetic (>12 keV) X-ray is mounted on a thick low Z ($Z \leq 6$) substrate. The artifact is easy to eliminate either by mounting the particle on a thin film or by mounting the particle on a higher Z substrate.

References

Chantler, C.T., Olsen, K., Dragoset, R.A., Chang, J., Kishore, A.R., Kotochigova, S.A. & Zucker, D.S. (2005). X-Ray Form Factor, Attenuation and Scattering Tables. Technical Report. Gaithersburg, MD: National Institute of Standards and Technology. Available May 1, 2007 at www.physics.nist.gov/ffast.

Compton, A. (1923). A quantum theory of the scattering of X-rays by light elements. *Phys Rev* **21**(5), 483–502.

Goldstein, J., Newbury, D., Joy, D., Lyman, C., Echlin, P., Lifshin, E., Sawyer, L. & Michael, J. (2003). *Scanning Electron Microscopy and X-Ray Microanalysis*. New York: Kluwer Academic/Plenum Publishers.

Klein, O. & Nishina, Y. (1928). The scattering of light by free electrons according to Dirac's new relativistic dynamics. *Nature* **122**, 398–399.

Knop, R.E. (1970). Random vectors uniform in solid angle. *Commum ACM* **13**, 326–327.

Markowicz, A. (2002). X-ray physics. In *Handbook of X-Ray Spectrometry*, Van Grieken, R. & Markowicz, A. (Eds.), pp. 1–94. New York, Basel: Marcel Dekker.

McMaster, W.H., Del Grande, N.K., Mallett, J.H. & Hubbell, J.H. (1969). Compilation of X-ray cross sections. Lawrence Livermore National Laboratory Report UCRL-50174 (section I 1970, section II 1969, section III 1969 and section IV 1969), University of California.

Ritchie, N.W.M. (2010). Spectrum simulation in DTSA-II. *Microsc Microanal* **15**, 454–468.

Salvat, F., Fernandez-Varea, J.M. & Sempau, J. (2009). PENELOPE-2008: A code system for Monte Carlo simulation of electron and photon transport. NEA no. 6416. Issy-les-Moulineaux, France: Organisation for Economic Co-operation and Development, Nuclear Energy Agency.

Uriano, G.A. (1981). Standard Reference Material U-900. National Bureau of Standards Certificate of Analysis. Available at www-s.nist.gov/srmors/certificates/archive/U-900.pdf.

Wilson, A.R. & Lambrianidis, L.T. (1990). Compton-scattering X-ray artifacts observed in an STEM with high take-off angle EDS detector. *J Microsc-Oxford* **160** (Pt 1), 1–7.